Computational Study of Flow and Heat Transfer in a Sudden Expansion Channel with Inclined Obstacles

Khudheyer S. Mushatet
College of Engineering
Thi-qar University

Qais A. Rishak
College of Engineering
Basrah University

Mohsen H. Fagr
College of Engineering
Thi-qar University

Abstract

The laminar flow through an obstacled sudden expansion channel is numerically investigated. Rectangular adiabatic inclined obstacles mounted behind the expansion region on the upper and lower wall of the channel were used. The effects of obstacles inclination angle, obstacles length, obstacles thickness and the number of obstacles on the flow and thermal fields for different Reynolds number and expansion ratio were examined. The angle of obstacles inclination was taken in the direction of streamwise flow and ranged from 30° to 90°. Three values of expansion ratio(ER=H/h) equal to 1.5, 1.75 and 2 were used. The choice of values of Reynolds number takes the consideration of symmetry state. The body fitted coordinates system is used to transfer the considered physical problem to computational domain in order to treat the complexity arising from applicable the boundary conditions near the inclined obstacles. The governing stream-vorticity equations expressed in generalized coordinates system were transformed to algebraic equations by using finite difference method. The solution of these equations was done by iteration method. The obtained results showed that there is a significant effect of obstacles angle on the hydrodynamic characteristics. The performed tests of the present results with related published results showed that there is an acceptable agreement.

Key words Sudden expansion channel, Laminar flow, Obstacles.

الخلاصة

اجريت في هذا البحث دراسة عددية لجريان طباقي خلال قناة ذات توسع فجائي مزودة بعوائق مستطيلة المقطع، مائلة ومعزولة تمت اضافتها الى المجرى في منطقة التوسع على الجدارين العلوي والسفلي بصورة متناظرة. يهدف البحث الى معرفة مدى تأثير زاوية ميلان هذه العوائق وطولها وسمكها بالاضافة الى عددها على الخصائص الحركية والحرارية للجريان ولقيم مختلفة من رقم رينولدز وكذلك لنسب باعية مختلفة. شمل البحث زوايا ميلان للعوائق من ٣٠° الى ٩٠° كما تم خلال البحث دراسة ثلاث نسب باعية هي ١.٥، ١.٧٥ وكذلك ٢. تم الاخذ بنظر الاعتبار بقاء الجريان متناظر عند اختيار قيم عدد رينولدز. استخدمت طريقة مواءمة الاحداثيات للجسم لتحويل المسألة محل البحث من الوسط الفيزياوي الطبيعي الى الوسط الحسابي لمعالجة التعقيد الناجم عن وجود العوائق المائلة. المعادلات الحاكمة للجريان والدوامية والمعبر عنها بنظام الاحداثيات المعمم تم تحويلها الى معادلات خطية من خلال طريقة الفروق المحددة ثم حلها بطريقة التكرار. النتائج التي اظهرها البحث بينت ان هناك تأثيرا ملحوظا لزاوية ميلان العوائق على الخصائص الحركية. اظهرت المقارنات التي اجريت لنتائج البحث الحالي مع نتائج الابحاث المنشورة مقبولية عالية للنتائج الحالية.

Introduction

The flow in a sudden expansion channels is encountered in many engineering applications. Although the flow is considered simple, the complexities arise due to the separation and reattachment after the expansion region. In recent studies, an increasing interest is focused on energy conservation systems. These systems include heat exchangers, cooling of electronic devices and solar collectors. The large number of previous studies focused on hydrodynamic and thermal behavior of the flow behind sudden expansion geometry. Therefore, non-published studies were done on using an inclined solid obstacles mounted behind the expansion region, and as a result, the effects of these obstacles on dynamic behavior of the flow and enhancement of heat transfer. The laminar flow of Newtonian fluid in planar and axisymmetric sudden expansion was studied by Scott et al. [1]. They covered the steady state flow at Reynolds number up to 200 and expansion ratio of 1.5, 2, 3 and 4. The results showed that the reattachment length and the eddy center location vary linearly with Reynolds number, but the relative eddy intensity was an exponential function of Reynolds number. Tao tang and Ingham [2] studied the steady laminar flow past a sudden expansion for incompressible fluid. The study covered Reynolds numbers up to 1000 and uniform inflow. The results showed that the eddy length increased linearly with Reynolds number for both small and large values of expansion ratios. Baloch et al. [3] investigated numerically the incompressible Newtonian flows through two and three dimensional expansions. The sudden expansion geometry had a square cross section. The obtained results show that for Reynolds number up to 10, a significant vortex activity was generated by fluid inertia giving recirculation zone and vortex enhancement. Battaglia et al. [4] performed numerical simulations and bifurcation calculations for flow of Reynolds number up to 200 in a two-dimensional sudden expansion channel. They found that the critical Reynolds number decreased with increasing expansion ratio. Thiruvengadam et al. [5] demonstrated the effects of flow bifurcation on temperature and heat transfer distributions in plane symmetric sudden expansion. They verified that the maximum Nusselt number that occurs on lower stepped wall is larger than the one that develops on the upper stepped wall and it develops near the side wall and not at the center of the duct. Battaglia and Papadopoulos [6] investigated experimentally and by two- and three-dimensional simulations the effect of three dimensionality flows of Reynolds number from 150 to 600 past 2:1 symmetric sudden expansion channel of 6:1 aspect ratio. They showed that when two-dimensional simulations were performed using the effective expansion ratio, the new results agreed well with the three-dimensional simulations and the experiments. The laminar flow through an axisymmetric sudden expansion using real-time digital particle

image velocimetry was studied by Hammed et al. [7]. They verified that the reattachment length and redevelopment length downstream of reattachment were linear functions of Reynolds number. The steady bifurcation phenomena for three dimensional flows through a plane–symmetric sudden expansion was investigated numerically by Chiang et al [8]. They showed that the bifurcation was dependent on flow Reynolds number, channel aspect ratio and expansion ratio. Simulations of three dimensional laminar forced convection in a plane symmetric sudden expansion were performed by Nie and Armaly [9]. They verified that the maximum Nusselt number was located inside the primary recirculation flow region and its location did not coincid with swirling flow impingement. The laminar incompressible flow in a symmetric plane sudden expansion was studied numerically by Wahba [10] where different iterative solvers on calculation of the bifurcation point were tested. He verified that the type of inflow velocity profile, whether uniform or parabolic has a significant effect on the onset of bifurcation. In the present work, a computational study has been made to study the dynamic of the flow behavior and thermal field in an obstacled sudden expansion channel. Inclined solid obstacles were mounted on upper and lower wall of the channel after the expansion region. The obstacles were inclined towards the flow stream. Different values of angle of inclination (AOI) $30° \leq AOI \leq 90°$ were used. The angle of inclination of obstacles, obstacles length and number of obstacles are studied for different values of Reynolds number and expansion ratio. The symmetry state is considered. The aim of the present study is to show the effect of inclined obstacles mounted behind expansion region on the flow behavior and thermal field.

1. Model description

The considered physical model is shown in Fig.1. It represents the upper half of plane symmetric sudden expansion. The upstream height is (h) and the downstream height is (H). The geometry provides a configuration within expansion ratio (ER=H/h) equals to 1.5, 1.75 and 2. The assumed fully developed flow at inlet leads to reduce the upstream length (L1) to be equal to the upstream height (h). The downstream length (L2) equals to 14 times the upstream height is considered where the effect of obstacles is vanished. The insulated obstacles were mounted symmetrically on the upper and lower walls of the expansion region and equal distance (l) between the obstacles was considered. The number of obstacles is varying as 1 and 3. Three obstacle lengths (Lo) equal to 0.1H, 0.15H and 0.2H and three obstacles thickness (th) equal to h/24, h/12 and h/6 were studied. Three values of angles of inclination (AOI) equal to 30°, 60° and 90° were examined. Different values of Reynolds

number (Re = 50, 100, 150 and 200) were selected taking by consideration the achievement of symmetric flow conditions.

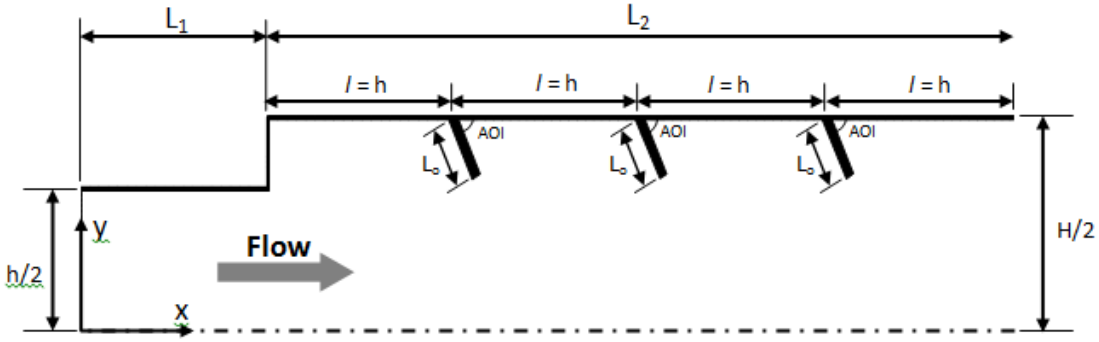

Fig.1 Schematic diagram of the considered problem

2.1. Mathematical model

The continuity, Navier–Stokes and energy equations for two dimensional steady state incompressible flow are described below by using the stream function - vorticity formulation after adopting the following assumptions:

- Fully developed at inlet.
- Constant thermo physical properties of the working fluid (air).
- Non-slip flow.
- Constant temperature at the expansion region walls.

Continuity equation:

$$\frac{\partial u}{\partial x}+\frac{\partial v}{\partial y}=0 \qquad (1)$$

Momentum equation in x-direction:

$$\frac{\partial u}{\partial t}+u\frac{\partial u}{\partial x}+v\frac{\partial u}{\partial y}=\upsilon\left(\frac{\partial^2 u}{\partial x^2}+\frac{\partial^2 u}{\partial y^2}\right)-\frac{1}{\rho}\frac{\partial p}{\partial x} \qquad (2)$$

Momentum equation in y-direction:

$$\frac{\partial v}{\partial t}+u\frac{\partial v}{\partial x}+v\frac{\partial v}{\partial y}=\upsilon\left(\frac{\partial^2 v}{\partial x^2}+\frac{\partial^2 v}{\partial y^2}\right)-\frac{1}{\rho}\frac{\partial p}{\partial y} \qquad (3)$$

Energy equation:

$$\frac{\partial T}{\partial t}+u\frac{\partial T}{\partial x}+v\frac{\partial T}{\partial y}=a\left(\frac{\partial^2 T}{\partial x^2}+\frac{\partial^2 T}{\partial y^2}\right) \qquad (4)$$

Differentiate Eq. (2) with respect to y and Eq.(3) with respect to x and then subtract Eq. (2) from Eq. (3) and rearrange the result:

$$\frac{\partial}{\partial t}(\frac{\partial v}{\partial x}-\frac{\partial u}{\partial y})+\frac{\partial u}{\partial x}(\frac{\partial v}{\partial x}-\frac{\partial u}{\partial y})+\frac{\partial v}{\partial y}(\frac{\partial v}{\partial x}-\frac{\partial u}{\partial y})+u\frac{\partial}{\partial x}(\frac{\partial v}{\partial x}-\frac{\partial u}{\partial y})$$
$$+v\frac{\partial}{\partial y}(\frac{\partial v}{\partial x}-\frac{\partial u}{\partial y})=\upsilon\left[\frac{\partial^2}{\partial x^2}(\frac{\partial v}{\partial x}-\frac{\partial u}{\partial y})+\frac{\partial^2}{\partial y^2}(\frac{\partial v}{\partial x}-\frac{\partial u}{\partial y})\right] \quad (5)$$

from the definitions of stream function and vorticity:

$$d\varphi = udy - vdx \quad (6)$$

$$\Omega=\frac{\partial v}{\partial x}-\frac{\partial u}{\partial y} \quad (7)$$

So, the governing equations will be:

$$\frac{\partial^2\varphi}{\partial x^2}+\frac{\partial^2\varphi}{\partial y^2}=-\Omega \quad (8)$$

$$\frac{\partial\Omega}{\partial t}+\frac{\partial\varphi}{\partial y}\frac{\partial\Omega}{\partial x}-\frac{\partial\varphi}{\partial x}\frac{\partial\Omega}{\partial y}=\upsilon\left(\frac{\partial^2\Omega}{\partial x^2}+\frac{\partial^2\Omega}{\partial y^2}\right) \quad (9)$$

$$\frac{\partial T}{\partial t}+\frac{\partial\varphi}{\partial y}\frac{\partial T}{\partial x}-\frac{\partial\varphi}{\partial x}\frac{\partial T}{\partial y}=a\left(\frac{\partial^2 T}{\partial x^2}+\frac{\partial^2 T}{\partial y^2}\right) \quad (10)$$

The above equations are dimensionlessed via using the following parameters :

$$X=\frac{x}{h}\ ,\quad Y=\frac{y}{h}\ ,\quad U=\frac{u}{u_\circ}\ ,\quad V=\frac{v}{u_\circ}\ ,\quad \psi=\frac{\varphi}{hu_\circ}\ ,\quad \tau=\frac{u_\circ t}{h}\ ,\quad \omega=\frac{\Omega h}{u_\circ}\ ,\quad \theta=\frac{T-T_\circ}{T_w-T_\circ}$$

So, equations (8-10) will become :

$$\frac{\partial^2\psi}{\partial X^2}+\frac{\partial^2\psi}{\partial Y^2}=-\omega \quad (11)$$

$$\frac{\partial\omega}{\partial\tau}+\frac{\partial\psi}{\partial Y}\frac{\partial\omega}{\partial X}-\frac{\partial\psi}{\partial X}\frac{\partial\omega}{\partial Y}=\frac{1}{\mathrm{Re}}\left(\frac{\partial^2\omega}{\partial X^2}+\frac{\partial^2\omega}{\partial Y^2}\right) \quad (12)$$

$$\frac{\partial\theta}{\partial\tau}+\frac{\partial\psi}{\partial Y}\frac{\partial\theta}{\partial X}-\frac{\partial\psi}{\partial X}\frac{\partial\theta}{\partial Y}=\frac{1}{\mathrm{Re}\,\mathrm{Pr}}\left(\frac{\partial^2\theta}{\partial X^2}+\frac{\partial^2\theta}{\partial Y^2}\right) \quad (13)$$

2.2. Grid generation

Due to presence of inclined obstacles, the physical domain becomes non-rectangular. So a suitable treatment for obstacles boundary conditions is needed to capture the inaccuracy arises for imposing a rectangular domain on this complex boundary. The grid generation method proposed by Thompson [11] is used to map the non- rectangular grids in physical domain into rectangular one in computational space. The most popular partial differential equation used for any complex-shaped bodies in two dimensional zone is an elliptic poison equation:

$$\zeta_{xx} + \zeta_{yy} = P(\zeta, \eta) \quad (14)$$

$$\eta_{xx} + \eta_{yy} = Q(\zeta, \eta) \quad (15)$$

Where P and Q are known functions used for controlling the grids clustering. It is worth to mention here that the grids adopted for the present work were generated at $P(\zeta, \eta) = Q(\zeta, \eta) = 0$.

This process is accomplished by addling the boundary conditions which specify ζ and η as functions of x and y. The dependent and independent variables are interchanged to produce a system of elliptic differential equations.

So, the governing equations, Eq. 11-13 will become:

$$\omega_\tau + \left(-\psi_\zeta \omega_\eta + \psi_\eta \omega_\zeta\right)/J = \left(\lambda\omega_\zeta + \sigma\omega_\eta + \alpha\omega_{\zeta\zeta} - 2\beta\omega_{\zeta\eta} + \gamma\omega_{\eta\eta}\right) / J^2 \,\mathrm{Re} \quad (16)$$

$$\theta_\tau + \left(-\psi_\zeta \theta_\eta + \psi_\eta \theta_\zeta\right)/J = \left(\lambda\theta_\zeta + \sigma\theta_\eta + \alpha\theta_{\zeta\zeta} - 2\beta\theta_{\zeta\eta} + \gamma\theta_{\eta\eta}\right) / J^2 \,\mathrm{Re}\,\mathrm{Pr} \quad (17)$$

$$\lambda\psi_\zeta + \sigma\psi_\eta + \alpha\psi_{\zeta\zeta} - 2\beta\psi_{\zeta\eta} + \gamma\psi_{\eta\eta} = -J^2\omega \quad (18)$$

Eq.16-18 are discretized by using finite difference scheme and then solved by iteration method with succesive over relaxation method (SOR).

2.3. Boundary conditions

In order to solve the mathematical model, the following boundary conditions were imposed On the upper wall:

$$\psi = 1 \quad , \quad \omega = \frac{-\alpha}{J^2}\psi_{\zeta\zeta} \text{ [12]} \quad , \quad \theta = 1$$

On the obstacles:

$$\psi = 1 \quad , \quad \omega = \frac{-\alpha}{J^2}\psi_{\zeta\zeta} \text{ [12]} \quad , \quad \frac{\partial\theta}{\partial n} = 0$$

Where n is a unit normal vector. On the symmetric line:

$$\psi = 0 \quad , \quad \frac{\partial\theta}{\partial Y} = 0$$

Fully developed conditions at inlet were imposed:

$$\frac{\partial\phi}{\partial X} = 0 \quad , \quad \psi = \psi(Y)$$

Where ϕ represents ψ, ω and θ.

At exit, to insure the smooth transition at the flow boundary, the following boundary conditions are used

$$\frac{\partial\psi}{\partial X} = 0 \quad , \quad \frac{\partial\omega}{\partial X} = 0 \quad , \quad \frac{\partial\theta}{\partial X} = 0$$

2.4.Grid dependency

To ensure that the hydrodynamic and thermal parameters are not affected by the mesh, different grid densities were examined for each expansion ratio ER. For ER = 1.5, the grid densities were (390×15), (390×30) and (600×45). For ER = 1.75, the grid densities were (390×21), (390×35) and (600×48). While for ER = 2, the grid densities were (390×30), (390×40) and (600×60). The results showed that increasing in grid density more than (390×30), (390×35) and (390×40) for ER = 1.5, 1.75 and 2 respectively has no significant effect on the results as shown in Fig.2 and Fig.3. So, these grid densities were selected in the present work.

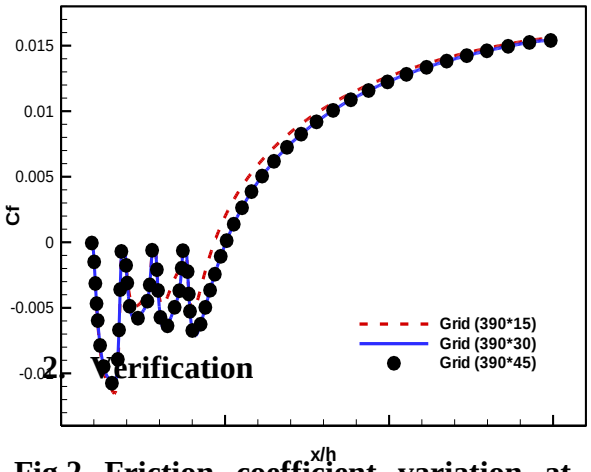

Fig.2 Friction coefficient variation at various grids at Re=150for ER=1.5, three obstacles, Lo=0.15H, th= h/24 and AOI=90°.

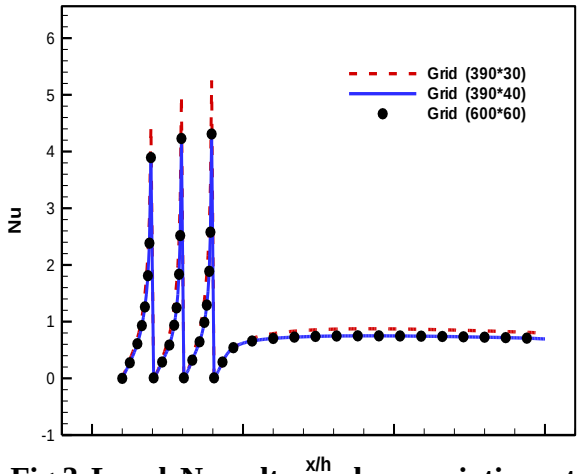

Fig.3 Local Nusselt number variation at various grids at Re=150for ER=2, three obstacles, Lo=0.2H, th= h/24 and AOI=60°.

2. Verification

3. Verification

To verify the present built home computer program, two tests were performed with related published results as show in Fig. 4 and Fig. 5. As the figures show, the comparison indicated an acceptable agreement.

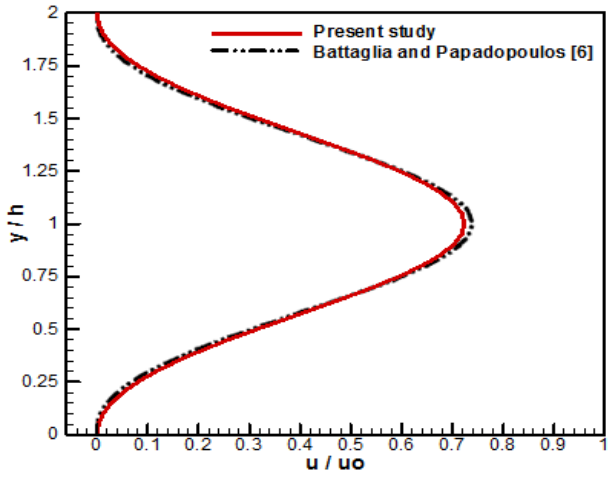

Fig.4 Comparison of present results of dimensionless streamwise velocity for ER=2 and x/h=4.5 at Re=171 with the predicted results of Battaglia and Papadopoulos [6].

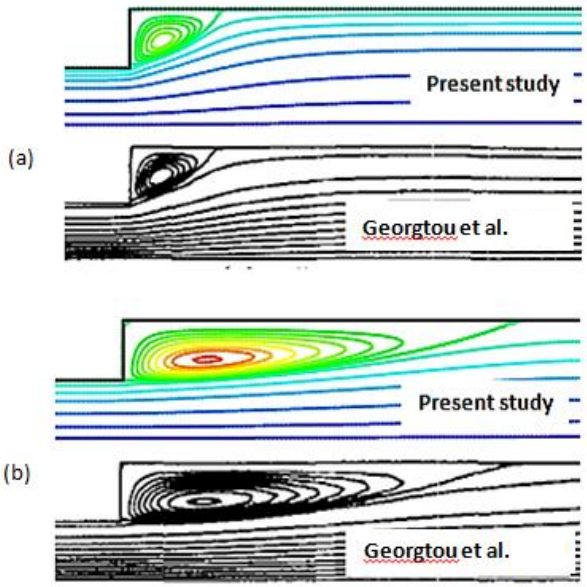

fig. 5 Comparison of present results of recirculation region for 2:1 expansion duct with the published results of Georgtou et al. [13].(a) Re =10. (b) Re =50.

4. Symmetry and asymmetry

fig.6 shows the streamwise velocity contours of flow at Re = 200 inside a channel of expansion ratio equals to 1.5 (case a), 1.75 (case b) and 2 (case c). This figure shows that at this Reynolds number, a two recirculation zones of equal size mounted symmetrically on upper and lower the centerline of the channel are developed. The streamwise velocity is primarily positive in the direction of flow except for the two recirculation zones that form immediately downstream of the expanding channel where the flow attaches the upper and lower walls. An effect of expansion ratio is that as it increases, the recirculation zone becomes larger at same Reynolds number due to the decreasing in the pressure drop. This effect can be seen by comparison cases a, b and c of fig.6.

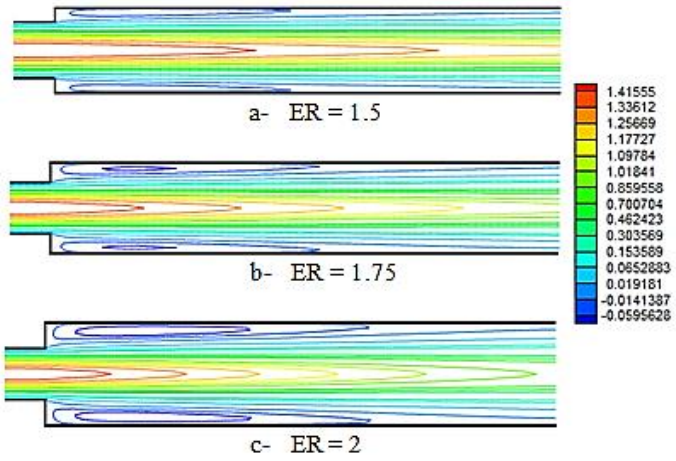

fig.6 Streamwise velocity distribution with symmetric flow pattern at Re=200.

The symmetry will disappear as Reynolds number accedes the critical Reynolds number as shown in fig.7 where the flow leaves the symmetric state (case a) to asymmetric state (case b) in which different sizes of recirculation zones are formed along the upper and lower walls. In this study, the symmetry state is taken in consideration which means that the values of studied Reynolds number will not accede 200.

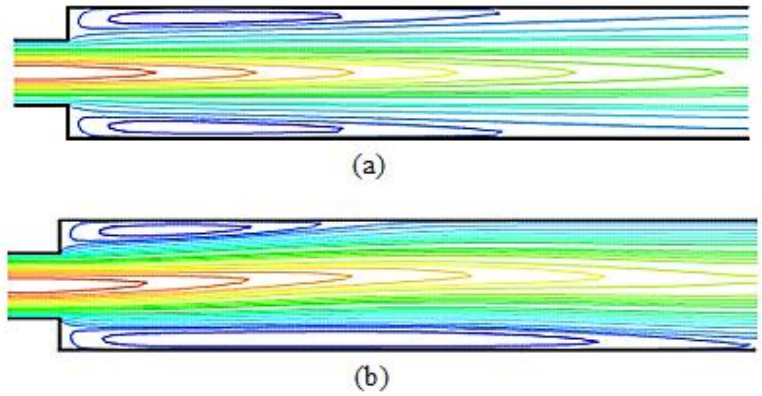

fig.7 Streamwise velocity contours for ER=2. (a) at Re = 200, (b) at Re =230.

5. Results and discussions

The two dimensional incompressible laminar flow in a sudden expansion obstacled channel has been numerically studied. Effects of number of obstacles, angle of inclination of the obstacles (AOI), length of obstacles (L_O) and Reynolds number (Re) on hydrodynamic and thermal parameters were tested for different expansion ratios.

5.1. Effects of number of obstacles on the hydrodynamic and thermal fields

The effect of number of obstacles on the flow structure at constant Reynolds number is shown in Fig. 8. The stream function contours and its recirculation zone for cases of no obstacles, one obstacle and three obstacles are shown. As the obstacles interrupt the development of the boundary layer, the recirculation zone downstream the obstacles is induced due to the flow separation. Therefore, increasing number of obstacles increases number of recirculation areas. The figure shows that the recirculation zone of the non obstacled channel develops to a longer zone of two recirculation areas created by adding one obstacle and by adding three obstacles, it becomes more longer with four recirculation areas.

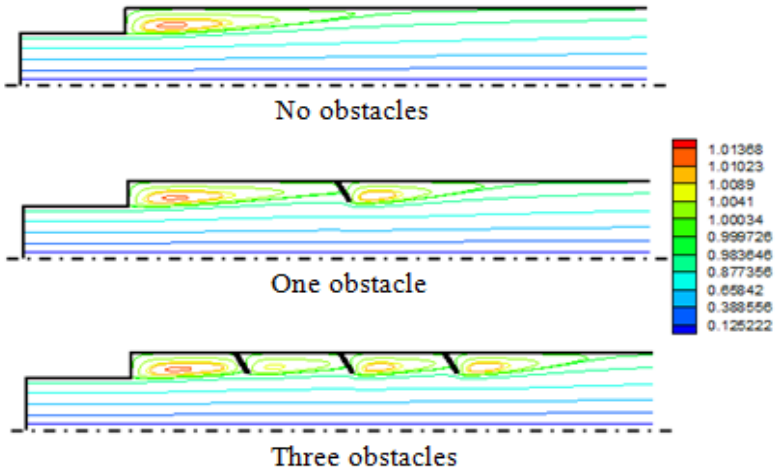

Fig. 8 Stream function contours at Re=150 for ER=1.5, L_O=0.15H and AOI=60°.

Fig.9 shows the effect of adding obstacles on the reattachment length. It is shown that the reattachment length is a linear function of the Reynolds number. It is also found that if the straight line representing reattachment length-Reynolds number relationship for not obstacled channel was to be extended, it will pass through the origin point. This trend is expected considering that the average shear rate at any chosen fixed streamwise distance normalized by the reattachment length is nearly constant [7]. Adding obstacles will remain the linear function of reattachment length-Reynolds number relationship but if it was to be extended, it will not pass through the origin. The extended line will shift to pass through a point represents the point of remote separation due to presence of obstacle. Note that the point of separation due to obstacle coincides with the free edge of the obstacle. Also, increasing number of obstacles increases reattachment length due to increasing flow separation.

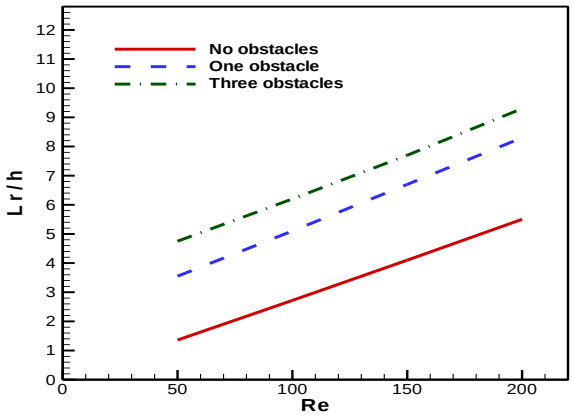

Fig. 9 Reattachment length-Reynolds number relationships for different obstacles number of AOI = 60° for ER = 1.75.

Fig.10 shows the average friction coefficient for the cases of different numbers of obstacles with respect to the Reynolds number. The friction coefficient changes its sign from negative to positive at the reattachment point. So, the longer recirculation region obtained by increasing number of obstacles will remain the negative sign friction coefficient for a longer axial distance. Therefore, the figure shows that average friction coefficient decreases by adding one obstacle, and more decreasing is shown by increasing obstacles number.

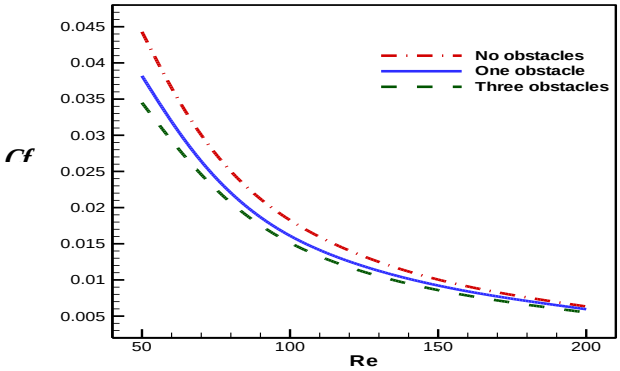

Fig. 10 Average friction coefficient at upper wall of expansion region with respect to Reynolds number for ER=1.5, L_O=0.15H and AOI=60°.

Fig. 11 represents the contours of dimensionless temperature for different number of obstacles. As the figure shows, the zone of high fluid temperature lies in the obstacled channel. The cause arises to increase recirculation zones due to presence of obstacles which increase the mixing and heat losses.

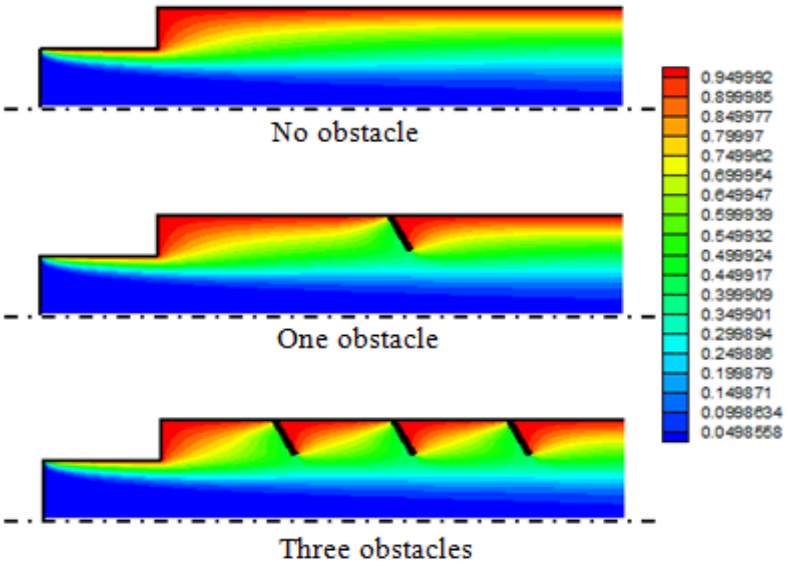

Fig. 11 Dimensionless temperature distribution at Re=150 for ER=1.75, L_O=0.2H and AOI=60°.

Fig. 12 shows the average Nusselt number variation with respect to the Reynolds number for cases of different obstacles number. As the obstacles number increases, the average Nusselt number increases. The increasing in the average Nusselt number is due to the intense mixing by the induced vortex.

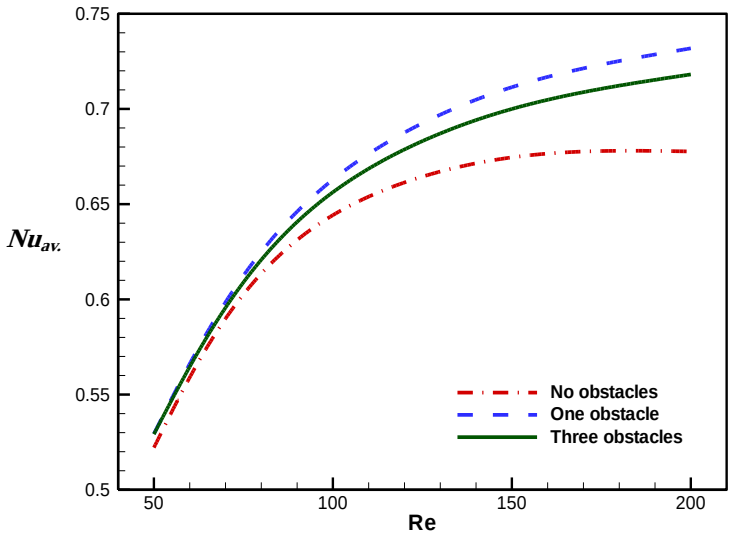

Fig. 12 Average Nusselt number at upper wall of expansion region with respect to Reynolds number for ER=2, L_O=0.2H and AOI=60°.

Table (1) shows the percentages increasing in the average Nusselt number when one and three obstacles are added comparing with case of non-obstacled channel.

Table (1) percentages increasing in the average Nusselt number for the case of ER = 1.5 with obstacles of L_O = 0.15H, th = h/6 and AOI = 90° at different Reynolds number.

No. of obstacles	Re = 50	Re = 100	Re = 150	Re = 200
1	32.503 %	25.712 %	23.219 %	21.852 %
3	59.284 %	51.203 %	47.947 %	46.133 %

5.2. Effects of the angle of inclination of obstacles on the hydrodynamic and thermal fields

The stream function distribution for different values of angle of inclination is seen in Fig. 13. As the figure shows, a vortex is observed downstream of the obstacles, which was induced due to the flow separation. The vortex was located close to the solid wall and its height was approximately equal to the extent of the flow blockage by the obstacles. The figure shows that the obstacles inclination angle has an effect on the area of the recirculation zone behind the obstacle. When the angle of inclination (AOI) increases from 30° to 60°, the recirculation zone becomes larger in its long and height. However, with further increment in AOI to 90°, it becomes smaller. The reason of this behavior is that the inclined obstacle will control the flow direction and as its angle increases from 30° to 60°, the flow toward duct center increases which enlarges the recirculation zone. But as its angle increases from 60° to 90°, the flow toward the duct center decreases compared with the flow toward the duct wall. However, the case of AOI =30° indicates the shortest recirculation zone.

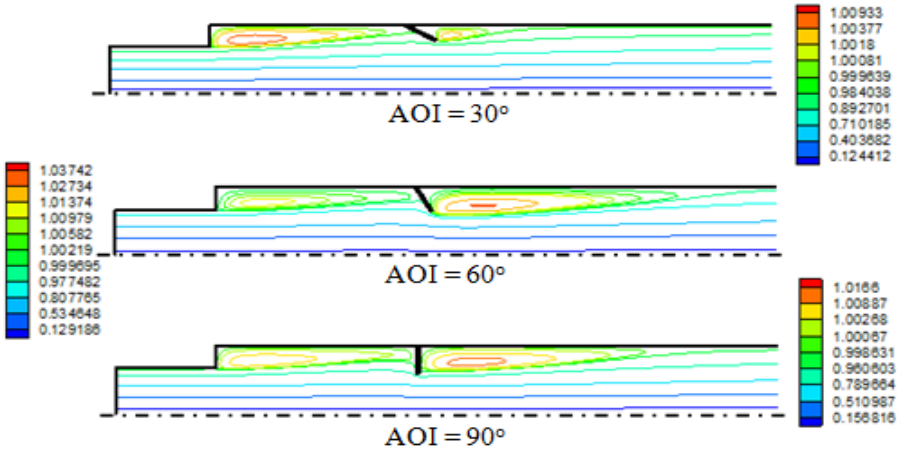

Fig. 13 Stream function contours at Re=150 for one obstacle case of ER=1.5 and L_O=0.2H.

Fig. 14 shows the effect of the angle of obstacles inclination on the reattachment length. Followed the separation behavior, it is shown that as the angle increases from 30° to 60°, the reattachment increases. But, as it increases from 60° to 90°, the reattachment length decreases but it remains larger than that for the case of 30°.

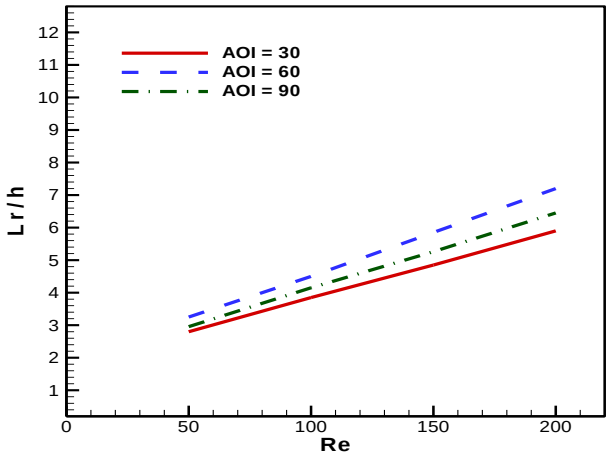

Fig. 14 Reattachment length for obstacled channels with one obstacle of L_O = 0.15H for ER = 1.75.

The effect of the obstacle inclination on the average friction coefficient ($C_{f\,av.}$) is shown in Fig. 15. It can be seen that the average friction coefficient for the case(AOI=60º) is less than that for other cases specially at low Reynolds number due to increasing in the recirculation region in which it still with negative sign for longer channel length.

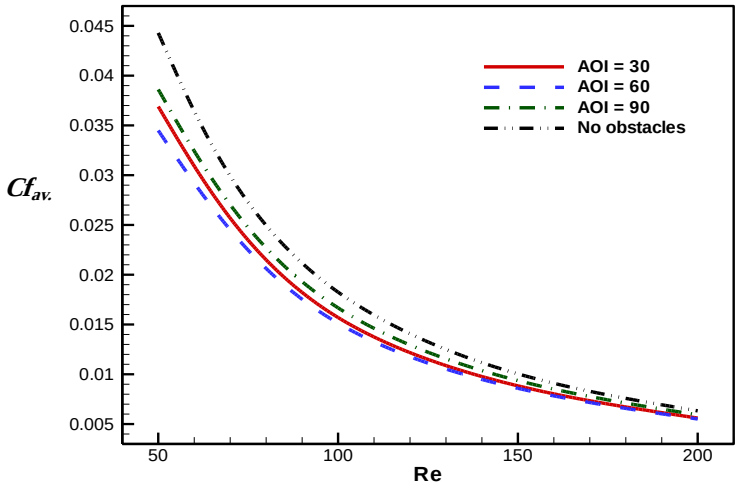

Fig. 15 Average friction coefficient at upper wall of expansion region for three obstacles case of ER=1.5 and L_O=0.15H.

Table (2) shows the percentages decreasing in the average friction coefficient when three obstacles of different inclination are added comparing with those of not obstacled channel.

Table (2) percentages decreasing in the average friction coefficient for the case of ER = 2, three obstacles of th = h/24 and L_O=0.15H at different Reynolds number.

AOI	Re = 50	Re = 100	Re = 150	Re = 200
30°	14.611 %	26.285 %	34.094 %	34.211 %
60°	16.712 %	28.936 %	45.140 %	50.712 %
90°	7.915 %	24.201 %	39.312 %	40.976 %

Fig. 16 shows the dimensionless temperature distribution for different values of obstacles inclination angles. Due to the higher improved mixing that obtained by increasing in the area of the recirculation zone when AOI = 60°, a better temperature distribution enhancement is seen.

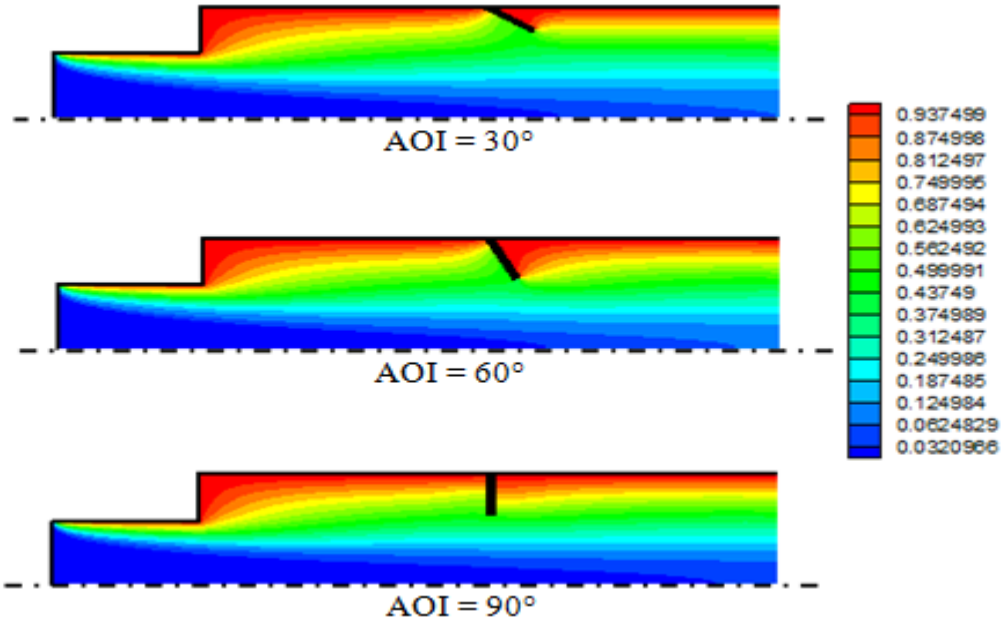

Fig. 16 Dimensionless temperature distribution at Re =100 for one obstacle case of ER=1.75 and L_O=0.2H.

The improvment in the Nusselt number by changing obstacles inclination angle can be seen in Fig. 17. This figure shows that the case of AOI = 60° obtains larger recirculation region, the average Nusselt number for this case has higher values as compared with other cases. Also, as Reynolds number increases, the difference between the average Nusselt number of different AOI cases increases as a result to the different increasing in the recirculation zones.

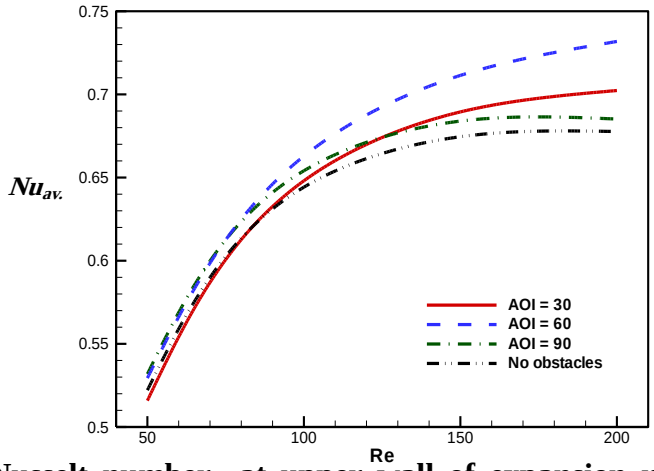

Fig. 17 Average Nusselt number at upper wall of expansion region with respect to Reynolds number for one obstacle case of ER=2 and L_O=0.2H.

5.3. Effect of obstacles length on the hydrodynamic and thermal fields

Fig. 18 shows the stream function contours with various inclined obstacles length L_O. It can be seen that more streamlines will separate due to increase the length of these obstacles which leads to increase the area of the recirculation zone downstream the obstacles as a result of the increasing in the pressure drop behind the obstacles.

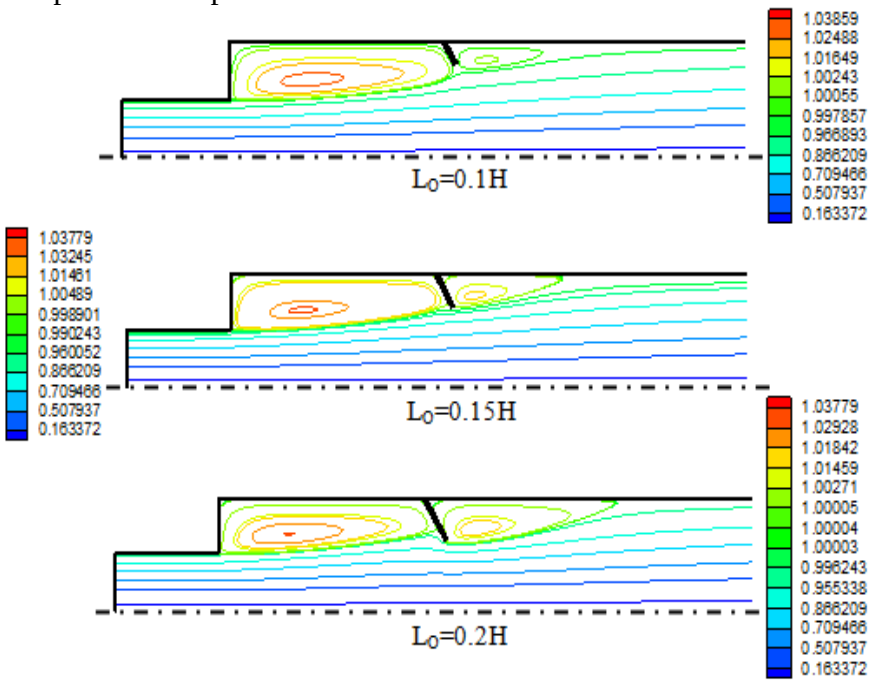

Fig. 18 Stream function contours at Re=50 for ER=2, one obstacle case and AOI=60°.

Fig. 19 shows the effect of obstacles length on the reattachment length. It is shown that as the obstacles length increases, the reattachment length increases due to increasing in the size of recirculation zone.

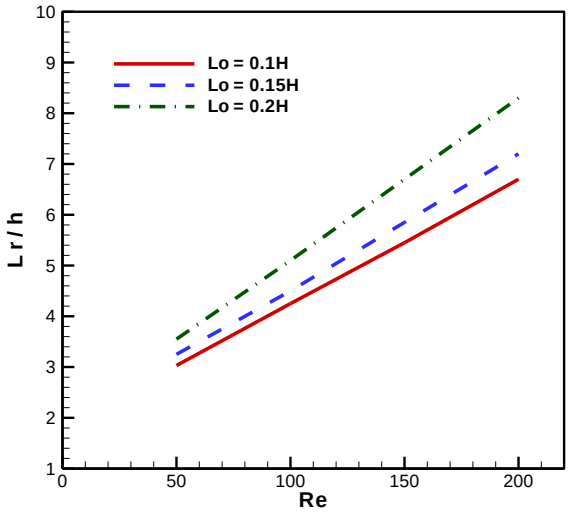

Fig. 19 Reattachment length-Reynolds number relationships for obstacled channels with one obstacle of AOI = 60° for ER = 1.75.

Fig. 20 shows the average friction coefficient for different inclined obstacle lengths with respect to the Reynolds number. As seen in this figure, the value of average friction coefficient for L_O=0.2H is lower than those of L_O=0.15H and 0.1H due to increase in the separation zone which leads the friction coefficient to remain with negative sign for longer channel length. Also, this figure shows that the dropping in average friction coefficient and its difference between the compared cases is decreased as the Reynolds number increases.

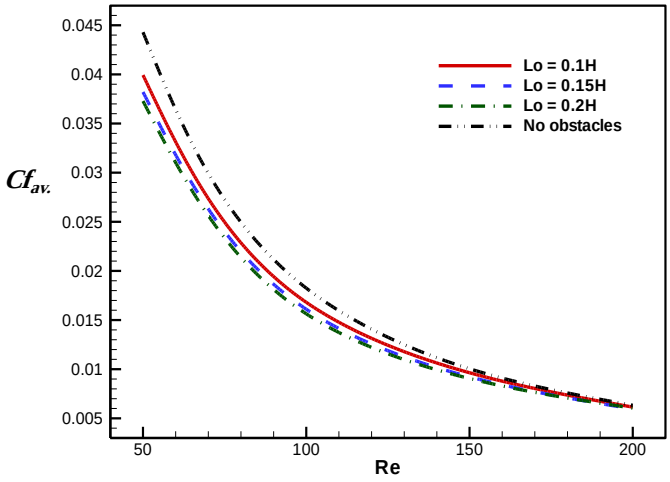

Fig. 20 Average friction coefficient at upper wall of expansion region with respect to Reynolds number for ER=1.5, one obstacle case and AOI =60°.

Table (3) shows the percentages decreasing in the average friction coefficient when three obstacles of different length are added comparing with those of non obstacled channel case.

Table (3) percentages decreasing in the average friction coefficient for the case of ER = 1.5, three obstacles of th = h/24 and AOI = 90° at different Reynolds numbers.

L_O	Re = 50	Re = 100	Re = 150	Re = 200
o.1H	7.123 %	4.301 %	2.887 %	3.542 %
0.15H	12.819 %	8.641 %	6.721 %	6.325 %
0.2H	15.031 %	13.934 %	13.203 %	12.001 %

Fig. 21 shows the dimensionless temperature distribution for cases of different inclined obstacle lengths (L_O). It is shown through this figure that the temperature distribution enhances as obstacle length increases specially at higher temperatures zone due to the improving in the fluid mixing.

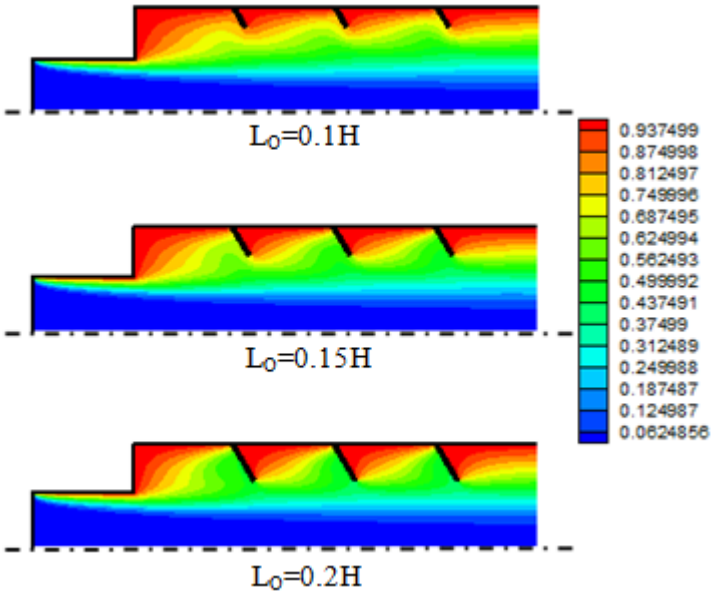

Fig. 21 Dimensionless temperature distribution at Re=200 for ER=2, three obstacle case and AOI=60°.

Fig. 22 shows the effect of obstacle length L_O on the average Nusselt number $Nu_{av.}$. It can be seen that that as the obstacle length increases, the average Nusselt number increases especially at higher Reynolds number. Also, there is a coincidence in the average Nusselt numbers for obstacles length L_O = 0.15H and L_O = 0.2H for (50≤ Re ≤100) is shown in this figure.

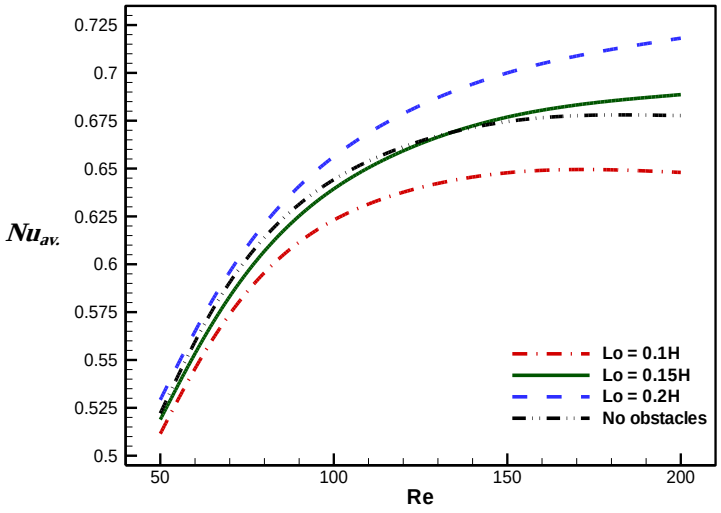

Fig. 22 Average Nusselt number at upper wall of expansion region with respect to Reynolds number for ER=2, three obstacles case and AOI =60°.

6. Conclusions

The laminar flow through a sudden expansion obstacled channel has been numerically analyzed. The obstacles were inclined towards the main flow stream. Different angles of inclination were tested as $30° \leq AOI \leq 90°$. The obstacles length (L_O) was changed as $0.1H \leq L_O \leq 0.2H$. The following conclusions can be obtained from the present study:

1- Increasing number of obstacles leads to decrease the friction coefficient and increase Nusselt number.

2- Increasing angle of inclination towards the main stream increasing the average rate of heat transfer. However, this increasing continues till AOI = 60° after that the rate of heat transfer decreases. The maximum values of average Nusselt number were noticed at AOI = 60°.

3- Increasing obstacles length leads to increase the rate of heat transfer and decrease the friction coefficient for all the studied angles of inclination.

4- Adding obstacles will shift the straight line that represents the reattachment length-Reynolds number relationship to pass through a point represents the point of remote separation.

7. Nomenclature

$C_{f\,av.}$ - Average coefficient of friction, [-]
ER - Expansion ratio (= H / h), [-]
H - Dimensionless downstream Channel height, [-]
h - Dimensionless upstream Channel height, [-]
J - Jacobian of direct transformation
$Nu_{av.}$ - Average Nusselt number, [-]
Re - Reynolds number(=Uh/ν), [-]
X ,Y - Dimensionless coordinates, [-]
ζ , η - computational domain coordinates
φ - stream function, [m^2/s]
ψ - dimensionless stream function, [-]
Ω - vortisity, [1/s]
ω - dimensionless vortisity, [-]
θ - dimensionless temperature, [-]

Pr - prandle number, [-]
T - temperature, [k]
U - Dimensionless streamwise velocity, [-]

α, β, γ – Transformation parameters
σ, λ - Geometrical parameters

References

[1] Scott P. S., Mirza F. A., Vlachopoulos J., A finite element analysis of laminar flows through planar and axisymmetric abrupt expansions, Computers and Fluids vol. 14, No. 4, pp. 423-432, (1986).

[2] Tao Tang, Ingham D. B., Multigrid solutions of steady two-dimensional flow past a cascade of sudden expansions, Computers and Fluids vol. 21, No. 4, pp. 647-660, (1992).

[3] Baloch A., Townsend P., Webster M. F., On two and three dimensional expansion flows, Computers and Fluids vol. 24, No. 8, pp. 863-882, (1995).

[4] Battaglia Francine, Simon J. Tavenery, Anil K. Kulkarniz, Charles L. Merkle, Biforcation of low Reynolds number flows in symmetric channels, American Institute of Aeronautics and Astronautics, (1996).

[5] Thiruvengadam M., Nie J. H., Armaly B.F., Bifurcated three-dimensional forced convection in plane symmetric sudden expansion, International Journal of Heat and Mass Transfer 48, pp. 3128–3139, (2005).

[6] Battaglia Francine, George Papadopoulos, Bifurcation Characteristics of Flows in Rectangular Sudden Expansion Channels, Journal of Fluids Engineering, Vol. 128 / pp. 671-679, (2006).

[7] Hammad K. J., Otugen M. V., Arik E. B., A PIV study of the laminar axisymmetric sudden expansion, Flow Experiments in Fluids 26, pp. 266-272, (1999).

[8] Chiang T. P., Tony W. H. Sheu, Robert R. Hwang, Sau A., Spanwise bifurcation in plane symmetric sudden expansion flows, Physical Review E,vol. 65, 016306, pp. 1-16, (2001).

[9] Nie J. H., Armaly B. F., Three-Dimensional Forced Convection in Plane Symmetric Sudden Expansion, Journal of Heat Transfer, Vol. 126 / pp. 836- 839, (2004).

[10] Wahba E.M., Iterative solvers and inflow boundary conditions for plane sudden expansion flows, Applied Mathematical Modeling 31, pp. 2553–2563, (2007).

[11] Thompson J. F., Thomas F., Mstia C. W., Automatic numerical generation of body fitted curvilinear coordinate system for field containing any number of arbitrary two dimensional bodies, J. Computational Physics, vol.15, pp. 299-319, (1974).

[12] Nagotov, E. F., "Application of numerical heat transfer" MCGraw Hill, (1978).

[13] Georgios C. Georgtou, William W. Schultz, Lorraine G. Olson, Singular finite elements for the problems sudden-expansion and the die-swell, International journal for numerical methods in fluids, Vol. 10, pp. 357-372 (1990).